

CHAPTER 1

BIOLOGICAL LATTICE GAS MODELS

Mark Alber ^{*}, Maria Kiskowski ^{*}, Yi Jiang [†], and Stuart Newman ⁺

^{*} *Department of Mathematics, 255 Hurley Building,
University of Notre Dame, Notre Dame, IN 46556-4618, USA
E-mail: malber@nd.edu*

[†] *Theoretical Division, Los Alamos National Laboratory
Los Alamos, NM 87545, USA
E-mail: yi@t7.lanl.gov*

⁺ *Department of Cell Biology & Anatomy, Basic Science Building
New York Medical College, Valhalla, NY 10595, USA
E-mail: stuart_newman@nymc.edu*

Modelling pattern formation and morphogenesis are fundamental problems in biology. One useful approach involves lattice gases (LGCA) systems. This paper reviews several stochastic lattice gas models for pattern formation in myxobacteria fruiting body morphogenesis and vertebrate limb skeletogenesis.

The formation of fruiting bodies in myxobacteria is a complex morphological process that requires the organized, collective effort of tens of thousands of cells. Myxobacteria morphogenesis provides new insight into collective microbial behavior since morphogenic pattern formation is governed by cell-cell interactions rather than of chemotaxis. An model is described for the aggregation stage of fruiting body formation.

Limb bud precartilaginous mesenchymal cells in micromass culture, undergo chondrogenic pattern formation which results in the formation of regularly-spaced "islands" of cartilage analogous to the cartilage primordia of the developing limb skeleton. An LGCA model is described for this process based on reaction-diffusion coupling and cell-matrix adhesion.

1. Introduction

Two main approaches have characterized mathematical modeling pattern formation (generation of specific arrangements of cells or other biological agents) and morphogenesis (generation of 3D forms from such agents) in

developmental biology. In the first, insight into basic mechanisms is sought by studying models based on simplified biological assumptions about cell behavior. The second approach involves attempts to build more comprehensive models and compare results of numerical simulations and biological experiments in detail. In this paper we will demonstrate both approaches by describing the modeling aggregation in *Myxobacteria* and the formation of chondrogenic patterns in limb cell cultures.

Mathematical and computational models of biological systems are by necessity extreme simplifications of a biological system. The purpose of a model is to capture the relevant aspects of a system being studied. Thus, a model is validated by its ability to capture the relevant behavior and make new predictions which may be empirically confirmed. Many examples of mathematical modelling applied to biological problems can be found in refs. ^{21,27}.

Models of biological problems fall into two categories: continuous models which use families of differential or integro-differential equations to describe “fields” of interaction and discrete models in which space, time or state may be discrete. Models may be deterministic or stochastic.

In biological applications, continuous models have been used to describe oceanic microbial cycles ⁴, microbial growth dynamics ⁵³, the spread of species through an ecosystem ⁵⁷, continuous biofilms ⁶², and periodic fungal or microbial structures ²⁶. (Many other examples of the use of PDEs in biological applications can be found in refs. ^{32,36,49}.) Equations in continuous models often describe fields of concentration or force and long-range interactions. For example, cells are often modeled as a density field and long-range chemotaxis is modeled as cell motion in response to a chemical field gradient.

Discrete models describe individual (microscopic) behaviors. They they are often applied to micro-scale events where a small number of elements can have a large (and stochastic) impact on a system. For example, while many periodic growth patterns can be modeled using continuous methods, modeling periodic growth patterns which depend sensitively on substrate concentration are best modeled with discrete methods ⁶⁴ including cellular automata (CA). The CA models and many others are reviewed in ref. ²⁰. Reference ³ also provides a good review of cellular automata applications in biology. ⁵² describes a cellular automata model for cell dispersion based on reaction and transport.

In lattice gas models, particles move freely on a spatial grid and undergo state changes when they collide. These state changes can be stochastic or

deterministic. Lattice gas models for fibroblast aggregation, ant trail organization and topographical neural maps are described in ref.²⁰. In classical lattice gases, there is an exclusion rule in which no two particles with the same orientation may occupy a node. Biological lattice-gas-based models may relax this exclusion principle.

While CA models are discrete in space, time and state, there are many approaches which include a combination of continuous and discrete model elements. For example, discrete subunits may interact with a continuously defined “field” (see, amongst others,³⁰). Coupled map lattices are discrete in space and time but have a continuous state space. Numerical methods commonly used to solve PDEs such as finite difference and finite elements methods are coupled map lattices. Lattice Boltzmann models are also coupled map lattices. Models in which state and space are discrete but time is continuous are called interacting particle systems.

This paper reviews several stochastic lattice gas cellular automata (LGCA) models for biological pattern formation. Section 2 provides general definition for LGCA and discusses the suitability of these models for describing biological pattern formation related to morphogenesis. LGCA are especially suited for modeling biological problems due to their versatility and the ease in which they may be defined and forward-evaluated. Their disadvantages are that they may require significant computer resources and sometimes are difficult to analyze.

Developmental morphogenesis is the molding of living tissues during development, regeneration, wound healing, and disease. It is a complex phenomenon involving gene regulation, changes in cell shape, cell-cell interactions, and cell division, growth and migration. Representing cell shape realistically is an important problem in modeling morphogenesis. An original method of cell representation consistent with lattice gas models is described in Subsection 3.2. In this method, particles may interact over a biologically-relevant geometric region but may be moved without violating the exclusion principle. This “template-based” approach is an efficient and generally applicable method for representing cells of any size, shape and orientation. Subsection 3.3 describes the cellular Potts model of Glazier and Graner²³ which is a more sophisticated representation of cell shape.

Our general approach is demonstrated in Sections 4 and 5 by describing modeling aggregation stage of fruiting body formation in *Myxobacteria* and pattern formation of precartilaginous cells in chick limb cell cultures. Each section includes a discussion of the choice and justification of the local rules for state evolution as well as an analysis of the novel properties of the

models and comparison with experimental data.

2. Lattice Gas Models

With the availability of new computational techniques in combination with large scale computing facilities, *in silico* experiments are becoming more and more an important option, in addition to *in vivo* and *in vitro* experiments, to study pattern formation in biological systems. Lattice gas cellular automata (LGCA) have become a rather popular and extremely flexible modelling tool in this context. (For a review see ^{3,20,16,40}.)

Cellular automata (CA) consist of discrete agents or particles, which occupy some or all sites of a regular lattice. These particles have one or more internal state variables (which may be discrete or continuous) and a set of rules describing the evolution of their state and position. Both the movement and change of state of particles depend on the current state of the particle and those of neighboring particles. Again, these rules may either be discrete or continuous (in the form of ordinary differential equations (ODEs)), deterministic or probabilistic. Updating can be synchronous or stochastic (Monte-Carlo).

In 1973 Hardy, de Passis and Pomeau ²⁵ introduced models to describe the molecular dynamics of a classical lattice gas (hence “Hardy, Passis and Pomeau” (HPP) models). They designed these models to study ergodicity-related problems and to describe ideal fluids and gases in terms of abstract particles. Their model involved particles of only one type which moved on a square lattice and had four velocity states. Later models extended the HPP in various ways and became known as lattice gas cellular automata (LGCA). LGCA proved well suited to problems treating large numbers of uniformly interacting particles.

LGCA employ a regular, finite lattice and include a finite set of particle states, an interaction neighborhood and local rules which determine the particles' movements and transitions between states ¹⁶. LGCA differ from traditional CA by assuming particle motion and an exclusion principle. The connectivity of the lattice fixes the number of allowed velocities for each particle. For example, a nearest-neighbor square lattice has four non-zero allowed velocities. The velocity specifies the direction and magnitude of movement, which may include zero velocity (rest). In a simple exclusion rule, only one particle may have each allowed velocity at each lattice site. Thus, a set of Boolean variables describes the occupation of each allowed particle state: occupied (1) or empty (0). Each lattice site can then contain

from zero to five particles.

The transition rule of an LGCA has two steps. An interaction step updates the state of each particle at each lattice site. Particles may change velocity state, appear or disappear in any number of ways as long as they do not violate the exclusion principle. For example, the velocities of colliding particles may be deterministically updated, or the assignment may be random. In the transport step, cells move synchronously in the direction and by the distance specified by their velocity state. Synchronous transport prevents particle collisions which would violate the exclusion principle (other models define a collision resolution algorithm). LGCA models are specially constructed to allow parallel synchronous movement and updating of a large number of particles¹⁶.

LGCA can model a wide range of phenomena including the diffusion of ideal gases and fluids³³, reaction-diffusion processes¹⁰ and population dynamics⁵¹. For details about CA models in physics see¹¹ and specifically for lattice-gas models see^{65,7}. In their biological applications LGCA treat cells as point-like objects with an internal state but no spatial structure. Because living cells function as agents interacting according to set rules, LGCA particularly suit modeling collective cellular behaviors^{2,12,13,18,19}.

Extensions of LGCA used in biological applications; “biological LGCA”^{20,2} may relax the exclusion principle or incorporate novel modelling elements. The lattice-gas-based model for limb chondrogenesis described in Section 5 does relax the exclusion principle since more than one particle may diffuse in the same direction from a node at a single timestep.

To summarize, LGCA are inherently simple; their discrete nature makes them straightforward to implement by computer and they lend themselves to agent-based approaches which reflect the intrinsic individuality of cells. Local rules can be developed from a microscopic level phenomenon understanding which is direct and intuitive. LGCA provide an opportunity to study interactions and behaviors which are difficult to formulate as continuum equations.

General limitations of LGCA are: the difficulty of going from qualitative to quantitative simulations since backward evolution is difficult; the artificial constraints of lattice discretization; and the difficulty in interpreting the simulation outcomes. The patterns that may emerge from even simple rules can be so rich that determining whether the model has genuinely captured the relevant biological mechanisms is difficult. Also, in many cases there is no faster way to predict the outcome of a simulation than to run the simulation⁶⁴. Another major problem is detecting and avoiding artificial

behavior¹⁶, (for example, ‘checkerboard’ patterns) which result from the overly simple geometry or local rules.

3. Representing Cell Shape

In this section we describe several models for representing cell shape used in cell alignment, cell migration and cell aggregation. These are fundamental to the problem of morphogenesis.

3.1. Morphogenesis

Understanding morphogenesis is a significant and challenging biological problem. Morphogenesis is a general phenomenon describing the change of living tissues. The final morphological pattern achieved during development, regeneration, wound healing, or disease is the product of spatio-temporal feedback between interacting cells and the expression of their genes.

Although morphogenesis is highly complex, it appears to be guided by a number of common principles. Cell shape is important during morphogenesis because cells may lengthen or shorten, round up or elongate. Changes in cell shape may precede or follow changes in gene expression. Also, cell shape greatly affects the interaction of cells in cases where cells interact via specialized structures. For example, Myxobacteria are very elongated and interact by “C-signaling” only when their cell poles are in contact. Cell alignment is also an important factor in cell interaction. Sub-groups of cells often align within tissues. Cells with different orientations within a tissue may differentiate into different cells. For example, an ingrowing epithelial bud of the Wolfian duct triggers the formation of secretory tubules in the kidneys of mice⁶³. Development of the *Drosophila* retina is initiated by a morphogenetic wave as furrow develops across the eye disc epithelium⁴⁴. During morphogenesis, tissues may fold and invert which makes the problem of alignment more complex. Finally, morphogenesis requires the collaborative interaction and movement of many cells, so migration and aggregation are also important elements in morphogenesis.

3.2. Template-based Model

In classical LGCA each particle (cell) is dimensionless and is represented as a single occupied node on a lattice. Cells without dimension are untenable for a sophisticated model of morphogenesis. Cells may be very elongated and

cell polarity determines movement and interaction. Also, a realistic model of cell overlap and cell stacking is needed since interaction may occur only at specific regions of highly elongated cells and cell density is a critical parameter throughout morphogenesis.

Reference ⁸ suggested one way of resolving the problem of stacking by introducing a semi-three-dimensional lattice where a third z -coordinate gives the vertical position of each cell when it is stacked upon other cells. Paper ⁶⁰ has introduced a model of rod-shaped cells that occupy many nodes and have variable shape in her cellular automata model of streaming and aggregation in myxobacteria. These two models are not classical lattice gases since they do not incorporate synchronous transport along channels. In Subsection 3.2.1 we describe a novel way of representing cells which facilitates modeling variable cell shape, cell stacking and incomplete cell overlap while preserving the advantages of classical lattice gases; namely, synchronous transport and binary representation of cells within channels (e.g., a '0' indicating an unoccupied channel and a '1' indicating an occupied channel).

In a template-based model ^{1,2,3} cells are represented as (1) a single node which corresponds to the position of the cell's center (or "center of mass") in the xy plane, (2) the choice of occupied channel at the cell's position designating the cell's orientation and (3) a local neighborhood defining the physical size and shape of the cell with associated interaction neighborhoods. The interaction neighborhoods depend on the dynamics of the model and need not exactly overlap the cell shape. In the models for rippling and aggregation, the size and shape of the cell are defined as a $3 \times \ell$ rectangle, where ℓ is cell length. The cell width is greater than 1 to account for interaction in the vertical y direction. As ℓ increases, the cell shape becomes more elongated. A cell length of $\ell = 30$ corresponds to the 1×10 proportions of rippling *Myxococcus xanthus* cells ³⁷. Representing a cell as an oriented point with an associated cell shape is computationally efficient, yet approximates continuum dynamics more closely than assuming point-like cells. The cell stacking problem is also resolved, since overlapping cell shapes correspond to cells stacked on top of each other. This cell representation conveniently extends to changing cell dimensions and the more complex interactions of fruiting body formation.

3.3. Cellular Potts Model

The cellular Potts model (CPM) is a more sophisticated Monte Carlo model in which a single cell consists of a domain of lattice sites. Cell volume and shape are very realistically described with the CPM. Since each cell has a different index, a CPM with Q states is also known as a Q -state Potts model. In the early 1980s, Anderson, Grest, Sahni and Srolovitz used the Q -state Potts model to study cellular pattern coarsening in metallic grains⁵⁶.

The original Potts model dates from 1952⁵⁴ as a generalization of the Ising model to more than two spin states. Glazier and Graner²³ generalized the Potts model to the CPM to study the sorting of biological cells. In the CPM, transition probabilities between site states depend on both the energies of site-site adhesive and cell specific non-local interactions. The CPM represents different tissues as combinations of cells with different surface interaction energies and other properties. It describes other materials, like the extracellular matrix (ECM), as a generalized cell.

Cell adhesion, an example of local interaction, is essential to multicellularity. Experimentally, a mixture of cell types with different types and quantities of adhesion molecules on their surfaces will sort out into islands of more cohesive cells within lakes of their less cohesive neighbors. Eventually, through random cell movement, the islands coalesce²². The final patterns, according to Steinberg's Differential Adhesion Hypothesis (DAH)⁵⁹, correspond to the minimum of interfacial and surface energy. The DAH assumes that cell sorting results entirely from random cell motility and quantitative differences in the adhesiveness of cells and that an aggregate of cells behaves like a mixture of immiscible fluids. *In vitro*⁶ and *in vivo* experiments²⁴ have confirmed the soundness of the analogy.

In this model, cellular patterns result from competition between a minimization of some generalized functional of configuration, *e.g.*, surface minimization, and global geometric constraints. The model starts from a free energy, the Potts Hamiltonian \mathcal{H} :

$$\mathcal{H} = \sum_{\vec{i}, \vec{j}} [1 - \delta_{\sigma(\vec{i}), \sigma(\vec{j})}], \quad (1)$$

where σ has Q different values and δ is the coupling energy between two unlike indices. The summation is over neighboring lattice sites \vec{i} and \vec{j} . At each time-step, a lattice site is chosen at random and a new trial index is also chosen at random from one of the other $Q - 1$ spins. The probability of changing the index at the chosen lattice site to the new index is:

$$P = \begin{cases} 1 & \Delta\mathcal{H} \leq 0 \\ \exp(-\Delta\mathcal{H}/T) & \Delta\mathcal{H} > 0 \end{cases}, \quad (2)$$

where $\Delta\mathcal{H} = \mathcal{H}_{\text{after}} - \mathcal{H}_{\text{before}}$ denotes the difference between the total energy before and after the index reassignment, and T is the temperature. This approach has been recently used for modeling development of a chicken limb bud ³⁰.

4. Model of Aggregation in Myxobacteria

Myxobacteria are one of the prime model systems for studying cell-cell interaction and cell organization of a uniform cell type preceding differentiation. Myxobacteria are social bacteria which swarm, feed and develop cooperatively ³⁵. When starved, myxobacteria self-organize into a three-dimensional fruiting body structure. Fruiting body formation is a complex multi-step process of alignment, rippling, streaming and aggregation that culminates in the differentiation of highly elongated, motile cells into round, non-motile spores. (See Fig. 4, from ⁴¹ with permission.)



Fig. 1. Snapshots during the fruiting body formation of *M. xanthus* at 0h, 12h, and 61h.

A successful model exists for the fruiting body formation of the eukaryotic slime mold *Dictyostelium discoideum* ^{31,45,46}. Understanding the formation of fruiting bodies in myxobacteria, however, would provide a new insight since collective myxobacteria motion depends not on chemotaxis as in *Dictyostelium* but on contact-mediated signaling (see ¹⁷ for a review).

In response to adverse conditions, free-roaming myxobacteria form multi-cellular aggregates called fruiting bodies. Aggregates range in size between 10 and 1,000 μm and are composed of 10^4 to 10^6 cells ⁵⁵. Within fruiting bodies, myxobacteria cells differentiate into resistant myxospores.

During aggregation, myxobacteria cells are elongated with a 2:1 to 14:1 ratio (cells are typically 2 to 12 by 0.7 to 1.2 μm ⁵⁵) and they move on

surfaces by gliding along their long axis⁹. Several hours after the onset of aggregation, cells begin transmitting a membrane-associated signaling protein called *C-signal* via their cell poles³⁷. Repeated C-signaling between cells raises the level of C-signal by two signal amplification loops in the *act* pathway. Increasing threshold levels of C-signal induce aggregation⁵⁸ and sporulation respectively.

Canonically, models for bacteria aggregation (e.g. *E. Coli*⁶¹ and *Bacillus subtilis*^{48,5}), as well as amoebae aggregation (e.g. *Dictyostelium discoideum*^{5,47}), have been based on attractive chemotaxis (chemoattraction), a long range cell interaction. Initialization of chemotactic signals plays an important role in the initial position of aggregates and subsequent signaling biases cell motion towards developing aggregates⁶¹. In myxobacteria, however, aggregates appear to form without the aid of chemotactic cues¹⁷. Rather, myxobacteria fruiting body development is organized by short-range cell-cell interactions.

Computational models based on cell collisions, a non-chemotactic short-range interaction, were first applied to explain myxobacteria rippling patterns^{28,8,43,2}. A recent paper²⁹, has extended an earlier continuous model for rippling to include myxobacteria aggregation.

Our model¹ is complementary to the continuum model²⁹, and focuses on a two-stage aggregate formation via streams. This mechanism, based entirely on local cell-cell interactions, accounts for both initialization and formation of large stable aggregates in a two-stage process. First, aggregates appear in random positions and cells join aggregates by random walk. Second, the aggregates reorganize as cells redistribute by moving within transient streams connecting aggregates.

The model^{2,1}, of the type described in Section 3.2, is based on local rules by which cells turn preferentially in directions that increase their level of C-signaling.

Description of Local Rules

- (1) Our model employs a hexagonal lattice with periodic boundary conditions imposed at all four edges. Unit velocities are allowed in each of the six directions.
- (2) Cells are initially randomly distributed with density δ , where δ is the total cell area divided by total lattice area.
- (3) At each time-step, cells may turn 60 degrees clock-wise, 60 degrees counter-clockwise or stay in their current direction. We use a Monte

Carlo process to model turning probabilities which favor directions that maximize the overlap of C-signaling nodes at the head of a cell with the C-signaling nodes at the tails of other cells.

- (4) During the transport step, all cells move synchronously one node in the direction of their velocity by updating the positions of their centers.

Cells move on a hexagonal lattice with periodic boundary conditions in all directions. Unit velocities (*or channels*) are allowed in each of the six directions. Identical rod-shaped cells are modeled as 3×21 rectangles and assume a cell size of $1 \times 7 \mu\text{m}$. The model keeps track of the C-signal exchange neighborhood of each occupied node which defines the possible locations of head-to-end overlaps between C-signaling cells. The total C-signaling neighborhood for each cell is fourteen nodes; seven at each cell pole separated by one half a cell length from the cell center.

A cell first turns stochastically 60 degrees clock-wise or counter-clockwise, or stays in its current direction. The model favors directions that maximize the overlap of the C-signal exchange neighborhood at the head of a cell with the C-signal exchange neighborhood at the tails of neighboring cells. This rule causes cells to align, which is a simplification of the hypothesis that alignment induces C-signaling which further induces cell alignment. Then, all cells move synchronously one node in the direction of their velocity by updating the positions of their centers.

4.1. Simulation Results

Cells aggregate in distinctive stages in our simulations. During the first stage, cells turn from low density areas towards areas of slightly higher cell density. Initially randomly distributed cells condense into small stationary aggregates (Fig. 2 (a)). These aggregate centers grow and absorb immediately surrounding cells. Next, some adjacent stationary aggregates merge and form long, thin streams which extend and shrink dynamically on their own and in response to interactions with other aggregates (Fig. 2 (b)). In each stream cells move head-to-tail in either direction along the stream. These streams are transient and eventually disappear at later stages of the simulation, leaving behind a new set of larger, denser stationary aggregates which are stable over time (Fig. 2 (c)). Cells in a typical aggregate form an annulus of aligned cells tangent to a hollow center (Fig. 2(d)).

Figure 3 shows the details of stream formation from two interacting aggregates. Initial aggregates crowd as they grow. When the distance between aggregates is less than one cell length, they begin exchanging cells, and the

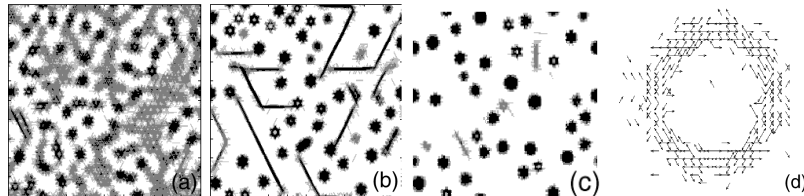


Fig. 2. Aggregation stages on a 500×500 lattice, which corresponds to an area of 2.8 cm^2 . Local cell density after (a) 200, (b) 900, and (c) 25,000 timesteps. Average cell density is 10. The number of simulated cells is 39,507. The darker shade of gray corresponds to higher cell density. (d) Directions of cell centers within a typical annular aggregate.

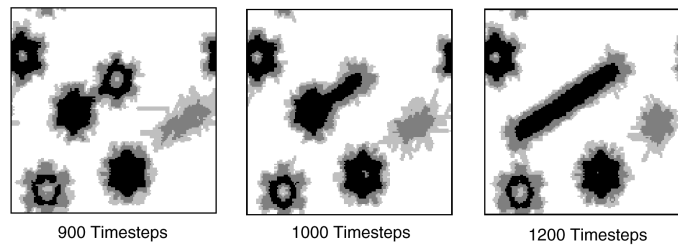


Fig. 3. The stream formation from two adjacent aggregates. Panels left to right correspond to 900, 1000, and 1200 timesteps, respectively. Lattice size is 128×128 .

cells reorganize into a stream. In contrast to stationary aggregates, cells travel long distances in streams.

A stream is bi-directional, with cells flowing equally in both directions along the stream. Given the end-to-end contacts required for C-signaling, an infinitely long stream of cells flowing in two directions is obviously a stable arrangement. However, there are a fixed number of cells within simulation streams, and thus streams are of finite length. Cells at the end of streams do not C-signal in the open space, hence will diffuse without any preferred direction. Although randomly diffusing cells often find their way back into the stream, some cells escape away from the stream. Over time, the stream shortens as it gradually loses cells. Fig. 4 (c) shows the path of a simulation stream in area-density phase space as it stochastically loses cells over time. A stream will lose cells more quickly if there is an aggregate near the end of the stream to absorb cells diffusing at the ends of the stream.

The eventual fate of a stream is to become a small stable aggregate. This occurs because a shortened stream is more sensitive to the noise caused by

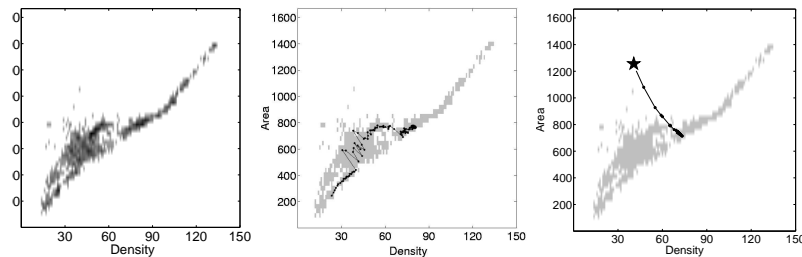


Fig. 4. Area-density phase diagram for (a) 186 stationary aggregates identified within two simulations over 25000 timesteps, (b) an initially small aggregate to which cells are slowly added over 1000 timesteps, and (c) an artificially constructed aggregate (star) over 600 timesteps. Relaxation of perturbation data in (b) and (c) are plotted every 10 timesteps on top of (a).

the cells freely diffusing at each end of the stream. After an abrupt and brief disordered transient state, the stream reorganizes into an aggregate. The area-density phase diagram Fig. 4 enables a prediction of the final aggregate shape based on the number of cells within the stream.

This diagram was obtained by plotting the areas and densities of every stationary aggregate which appeared over the course of two simulations. These aggregates fall within a narrow range in the area-density phase diagram shown in Fig. 4 (a), illustrating that for an aggregate of a given cell number, its area and density is prescribed within a narrow attractor region. In ¹ the stability of this attractor region is analyzed with respect to two kinds of noise: 1) external noise, including those in the initial random distribution of cells and our perturbations to the system; 2) internal noise, which originate from the stochastic nature of the cell's turning process.

In particular, a stable aggregate is perturbed in two ways. First, an adiabatic perturbation is studied by gradually adding cells to an initially small, isolated aggregate. As cells are slowly added, the aggregate increases in area and density while remaining within the attractor region (Fig. 4(b)). Second, a non-adiabatic perturbation is introduced by placing two duplicate aggregates in close proximity of each other, which creates a new aggregate with double the initial area and the same density. Over 600 timesteps, this aggregate gradually reorganizes so that it has an area and density within the stable region (Fig. 4(c)). Results from both kinds of perturbations suggest that this attractor region is a stable attractor in the area-density phase space of aggregates.

The area-density phase diagram not only prescribes the region of stable

aggregates, it also helps ones understanding of the formation of streams. When two stationary aggregates interact, the area of interacting cells increases at the moment of interaction while the density remains approximately the same. Thus, the newly formed aggregate lies off the attractor region. Large aggregates with high cell density and area will fuse and quickly form a new stationary aggregate as in Fig. 5. Smaller aggregates have a lower cell density and lower cell C-signaling levels, so when small aggregates fuse, they have a longer transient stage and are more likely to form a stream. Fig. 3 shows the formation of a stream from two interacting aggregates.

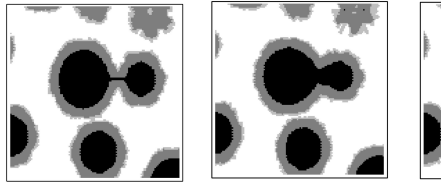


Fig. 5. Two large aggregates fuse via a submerged stream. Panels left to right correspond to 19000, 24000 and 26000 timesteps on a 128×128 lattice, respectively.

The model reproduces the unique structures of several Myxobacteria fruiting bodies. In *Myxococcus xanthus*, the basal region of the fruiting body is a shell of densely packed cells which orbit both clock-wise and counter-clockwise around an inner region only one-third as dense. A magnified picture of the cell centers of a typical aggregate in simulations show that cells are arranged in a dense, concentric layer tangent to a relatively low-density inner region (Fig. 2 (d)) and cell tracking shows that cells orbit either clockwise or anti-clockwise along the periphery of the orbit. Further, aggregates in our simulation often form in clusters of two or three closed orbits while in *Stigmatella erecta*, several fruiting bodies may form in groups and fuse⁵⁵.

In experiments, one Myxobacteria aggregate has been observed to mysteriously grow as an adjacent aggregate disappears³⁴. Our simulations offer a mechanism for this process: a stream may form connecting two adjacent aggregates and, following a C-signaling line of cells, cells stream from the smaller aggregate to the larger aggregate. Experimentally, these streams may not be visible if the density threshold for viewing cells is greater than the density found within the stream.

5. A Model for Chondrogenic Patterning

Chondrogenesis is the development of cartilage, which is a tough flexible tissue from which the skeleton of the limb and vertebral column is initially established during embryonic development. The cartilage skeleton of the limb develops as a series of spot-like and bar-like condensations of the precartilaginous cells. In these condensations the cells (also called "mesenchymal" cells), which are initially dispersed in a gel-like medium called the extracellular matrix (ECM), move closer to one another, making transient contact, which triggers their differentiation into cartilage. In species with bony skeletons, such as birds and mammals, the cartilage skeleton serves as a structural template which is later replaced by bone. In low volume, high density ("micromass") cultures of precartilaginous mesenchymal cells, depending on the culture medium and the limb-type origin of the cells (wing buds vs leg buds), patterns of condensations form which may be spot-like, stripe-like, or fully confluent (sheet-like).

This section presents a stochastic lattice gas model for the formation of patterns of mesenchymal condensations in micromass cultures. This *in vitro* system provides a simplified, experimentally tractable model for skeletal patterning in the vertebrate limb. Its quasi-2D geometry suits computational modeling particularly well (see Refs. ^{39,40} for details). For the computational model to be manageable one must select key processes from the hundreds of cell-cell and cell-gene product interactions in the limb. Our choice for the "core" set of patterning interactions described below comes from experiments performed on the limb-forming cells of several species.

Chondrogenesis in micromass culture can be described as follows. Over 36-72 hours in a controlled experiment, a homogeneously distributed population of undifferentiated limb bud mesenchymal cells cluster into dense islands, or "condensations," of aggregated cells ⁴². The roughly equally spaced patches of approximately uniform size are reminiscent of the patterns produced by the classical Turing reaction-diffusion mechanism. The condensations develop concurrently with increases in extracellular concentrations of a cell-secreted protein, fibronectin, a non-diffusing extracellular matrix macromolecule which binds adhesively to cell surface molecules, including receptors known as integrins, which can transduce signals intracellularly. The limb cells also produce the diffusible protein TGF- β , which positively regulates its own production as well as that of fibronectin ⁵⁰. In what follows, we describe a model for the production of fibronectin and subsequent limb bud patch formation using an LGCA-based reaction-diffusion

process having TGF- β as the activator but with an unknown inhibitor.

5.1. *Computational Model*

Our computational model contains three components.

First, we model cells as occupied nodes of a square lattice (i.e., a rectangular grid) whose default behavior is random walk diffusion (analogous to Brownian motion). We describe the diffusion of cells and other diffusing agents on the lattice, below. We assume all cells are identical.

Second, we simulate on the lattice a cell-driven process that depends on the interaction between two molecular species: a diffusible activator, A, which we identify with TGF- β in the developmental model, and an inhibitor, B, which we identify with the laterally-acting inhibitory activity in the developmental model. For the purpose of the computational model we make the assumption that B is a diffusible molecule, with a faster diffusion rate than A. Since cells produce these molecular species, only nodes of the lattice that contain cells produce morphogens.

Third, when cells encounter threshold levels of activator, they respond by producing a secreted, but otherwise immobile, molecular species to which cells attach. We term this substrate adhesion molecule (SAM) and identify it with fibronectin in the developmental model.

Our simulation defines a “morphogenic domain” on a square $n \times n$ lattice by an $n \times n$ matrix of 0s and 1s. A ‘0’ indicates a node outside of, and a ‘1’ indicates a node belonging to, the morphogenic domain. The domain, all portions of which need not be connected, and which can have holes, can freely change at each time step and could be calculated by an auxiliary program. The only restriction on the domain is that it is a union of overlapping rectangles of at least two lattice points in height and width. In the current simulations, the morphogenic domain is the entire $n \times n$ lattice. The components in the morphogenic domain of the lattice include cells, activator molecules, inhibitor molecules and SAM molecules. We store the concentration of each of these components as an $n \times n$ matrix of integers, where the matrix element (i,j) corresponds to the concentration of the various components at the node (i,j) .

Multiple cells and molecules of each type may occupy a node. Boundary conditions for the morphogenic domain of the lattice are reflective, so that particles (cells or molecules) cannot diffuse beyond the domain boundary.

We initially distribute a fixed number of cells uniformly on a disc-shaped region centered in the morphogenic domain of the lattice. We set initial

densities of activator, inhibitor and SAM to zero. The total number of cells remains constant throughout the simulation and cells secrete activator, inhibitor, and SAM molecules. Activator and inhibitor molecules diffuse through the morphogenic domain of the lattice at every time-step, while SAM diffuses only during the time-step in which it is secreted.

Simulation results that depict cells, represent SAM-attached cells as black pixels and unattached cells as gray pixels. This representation corresponds to the appearance of cells in micromass cultures visualized by Hoffman Modulation Contrast microscopy, where the rounded cells in condensations appear darker than the flatter cells outside the condensations.

5.2. *Simulation Results*

In this section we demonstrate comparison between simulation and experimental results by describing chemical peaks and cell clustering under standard “leg” conditions.

In living leg-cell cultures the initial cell distribution is homogeneous, but, by the second day of growth, cells begin to form tightly packed focal condensations. Spacing between condensations is irregular, with a measurable average distance between centers (i.e., the average peak interval). The average condensation size generally increases in wing-cell cultures as the condensations expand and often merge^{42,15}), whereas it stays fixed in leg-cell cultures where most condensations remain discrete^{14,15}. The terminal pattern in the leg cultures occurs around 3 days and in the wing cultures around 4 days. The condensations differentiate fully into cartilage nodules by day 6.

We initially explored the behavior of the CA model under conditions that simulate those of a typical limb- cell micromass culture. The initial micromass diameter *in vitro* is 3 mm. Although living cells in standard *in vitro* experiments are plated at greater than confluent density (see. e.g., Ref. 15), a layer of ECM rapidly separates the cells. Our simulations assumed a matrix to cell area ratio of 60:40, a cell diameter of 15 μ m, and a “culture” spot diameter of 120 cells. Thus we model cells with average density 1 on a disk 120 nodes in diameter (see Figure 6).

As cells diffuse, one or more cells, or no cells, may occupy a node, so the production of activator and inhibitor varies over the lattice. Peaks of morphogen A and B begin to appear early in the simulation. Morphogen A peaks are only 1 or 2 nodes in size and levels drop from over 1000 units in a peak to zero units in immediately surrounding nodes (Figure 6a). Mor-

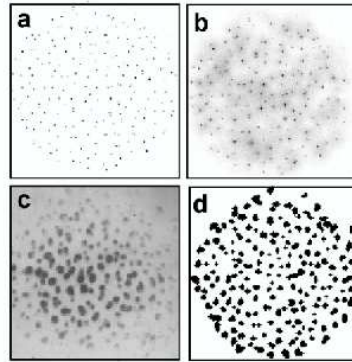


Fig. 6. Simulation results for scaled concentrations of key variables compared to the leg condensation pattern. (a) Morphogen A concentration, and (b) morphogen B concentration, after 4000 time-steps for control leg parameters; (c) Leg condensations visualized by Hoffman Contrast Modulation optics after 72 hours. Actual diameter of the circular culture is 3 mm (“low magnification view”); (d) Scaled SAM density after 4000 time-steps for control leg parameters. Simulations correspond to a low magnification view.

phogen B peaks are larger in size and much more diffuse (Figure 6b). For comparison, we show *in vitro* condensations at the scale of a full micro-mass culture for the comparable experimental stage (Figure 6c). When the level of morphogen A in the simulation reaches a threshold, the cells begin to deposit SAM (Figure 6d). Cells stick to these SAM deposits and local cell density increases. Activator, SAM and cell concentration peaks are all co-local (compare Figure 7 d, e and f).

Comparison of the development of condensations in experiments and simulations indicated that the period spanned by computational time-steps 1000-4000 corresponded to 50-72 hours in culture. In particular, the cell density distribution after 1000 time-steps for the optimized parameters qualitatively resembles precartilagel condensations after 50 hours. During the next 3000 times-steps the islands’ areas grow but their number remains unchanged, as in experiments after 72 hours.

Simulated morphogen peaks, SAM deposits and cell clusters develop in both time and space (Figure 7). The number of SAM deposits does not increase between 1000 and 4000 time-steps, indicating that almost all activator peaks form within 1000 time-steps. Activator peaks remain colocal with SAM deposits. SAM clusters grow, however, and occasionally fuse over 4000 time-steps (compare Figure 7 b and e).

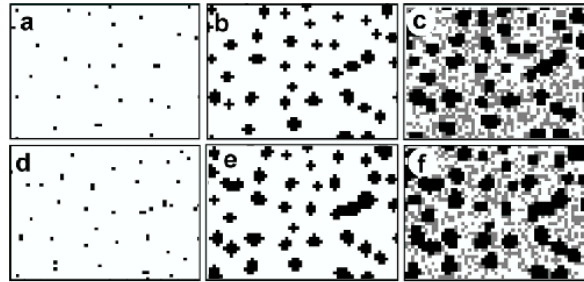


Fig. 7. Simulation dynamics of activator concentrations, SAM accumulation, and cell density over 1000 to 4000 time-steps for control parameters. (a) Morphogen A concentrations greater than threshold (1000 units), (b) SAM locations and (c) smoothed free (gray) and stuck (black) cell locations after 1000 time-steps. (d) Morphogen A concentrations greater than threshold (1000 units), (e) SAM locations and (f) smoothed free (gray) and stuck (black) cell locations after 4000 time-steps. Simulation images correspond to a high magnification view.)

The model was shown³⁹ to successfully determine a non-trivial parameter set that reproduces the number, size, and distribution of condensations of the standard culture, and demonstrate the ability of this parameter set to produce qualitatively accurate simulations of cultures under diluted, TGF- β -stimulated, reduced-inhibitor and fibronectin-transfected conditions. Therefore, the model captures important aspects of development.

Indeed, LGCA modeling as presented in³⁹, far from being a retrospective summary of existing experiments, is actually a parallel means of experimentation on systems with partially characterized relevant variables and parameters have been (e.g., chondrogenic patterning *in vitro*). It is an efficient and cost-effective tool for homing in on the range of potential manipulations that can provide decisive tests of *in vitro* and *in vivo* experimental models.

Acknowledgments

This work was supported by NSF Grant No. IBN-0083653 and by DOE under contract W-7405-ENG-36. We acknowledge support from the Center for Applied Mathematics and the Interdisciplinary Center for the Study of Biocomplexity at the University of Notre Dame.

References

1. M.S. Alber, Y. Jiang and M.A. Kiskowski, *Phys.Rev.Lett.* in press.
2. M.S. Alber, Y. Jiang, and M.A. Kiskowski, *Physica D* **191**, 343 (2004).
3. M.S. Alber, M.A. Kiskowski, J.A. Glazier and Y. Jiang, *On cellular automation approaches to modeling biological cells*, in J. Rosenthal and D.S. Gilliam (Eds.), *Mathematical Systems Theory in Biology, Communication, and Finance*, Springer-Verlag, New York, 2002, p. 1.
4. A.P. Belov, J.D. Giles, *Hydrobiologia* **349**, 87 (1997).
5. E. Ben-Jacob, I. Cohen, and H. Levine, *Advances in Physics* **49**, 395 (2000).
6. D. Beysens, G. Forgacs, and J. A. Glazier, *Proc. Natl. Acad. Sci. USA* **97**, 9467 (2000).
7. J. Boon., D. Dab, R. Kapral, and A. Lawniczak, *Physics Reports* **273**, 55 (1996).
8. U. Borner, A. Deutsch, H. Reichenbach, and M. Bar, *Phys. Rev. Lett.* **89**, 78101 (2002).
9. R.P. Buchard, *Annu. Rev. Microbiol.* **35**, 497 (1981).
10. S. Chen, S. P. Dawson, G. D. Doolen, D. R. Janecky, and A. Lawniczak, *Computers & Chemical Engineering* **19**, 617 (1995).
11. B. Chopard and M. Droz, *Cellular automata modeling of physical systems*, Cambridge University Press, NY, 1998.
12. A. Deutsch, *J. Biosc.* **24**, 115 (1999).
13. A. Deutsch, *Mathematical Biosciences* **156**, 255 (1999).
14. S.A. Downie, and S.A. Newman, *Dev. Biol.* **162**, 195 (1994).
15. S.A. Downie, and S.A. Newman, *Dev. Biol.* **172**, 519 (1995).
16. S. Dormann, *Pattern Formation in Cellular Automation Models*, Dissertation, Angewandte Systemwissenschaft FB Mathematik/Informatik, Universität Osnabrück, 2000.
17. M. Dworkin, *Microbiol. Rev.* **60**, 70 (1996).
18. L. Edelstein-Keshet and G.B. Ermentrout, *Contact response of cells can mediate morphogenetic pattern formation*, *Differentiation* **45** (1990), p. 147.
19. L. Edelstein-Keshet and G.B. Ermentrout, *J. Math. Biol.* **29**, 33 (1990).
20. G.B. Ermentrout and L. Edelstein-Keshet, *J. Theor. Biol.* **160**, 97 (1993).
21. C. Fall, E. Marland, J. Wagner, and J. Tyson (Eds.), *Computational Cell Biology: An Introductory Text on Computer Modeling in Molecular and Cell Biology*, Springer-Verlag, New York, 2002
22. G. Forgacs, R. Foty, Y. Shafir, and M. Steinberg, *Biophys. J.* **74**, 2227 (1998).
23. J. A. Glazier and F. Graner, *Phys. Rev. E* **47**, 2128 (1993).
24. D. Godt and U. Tepass, *Nature* **395**, 387 (1998).
25. J. Hardy, O. de Pazzis, and Y. Pomeau, *Phys. Rev. A* **13**, 1949 (1976).
26. F.C. Hoppensteadt and W.P. Jager, *A hysteresis model for bacterial growth patterns: modelling of patterns in time and space*, Springer-Verlag, Berlin, **55** (1984), p. 123.
27. F.C. Hoppensteadt, C.S. Peskin, *Modeling and simulation in medicine and the life sciences*, 2nd edition, Springer, Berlin, 2001.

28. O. Igoshin, A. Mogilner, D. Kaiser, and G. Oster, *Proc. Natl. Acad. Sci. USA* **98**, 14913 (2001).
29. O. Igoshin, R. Welch, D. Kaiser, G. Oster, *Proc. Natl. Acad. Sci. USA* **101**, 4256 (2004).
30. Izaguirre, J. A., Chaturvedi, R., Huang, C., Cickovski, T., Virtue, P., Thomas, G., Forgacs, G., Alber, M., Hentschel, G., Newman, S.A. and Glazier J.A., *Bioinformatics* **20**, 1129 (2004).
31. Y. Jiang, H. Levine, and J.A. Glazier, *Biophys. J.* **75**, 2615 (1998).
32. D.S. Jones and B. D. Sleeanhoopesman, *Differential Equations and Mathematical Biology*, CRC Press, Boca Raton, USA, 2003.
33. L. P. Kadanoff, G. R. McNamara, and G. Zanetti, *Phys. Rev. A* **40**, 4527 (1989).
34. D. Kaiser, private communication.
35. D. Kaiser and L. Kroos, in M. Dworkin and D. Kaiser (Eds.), *Myxobacteria II*, Am. Soc. Microbiol., Washington DC, 1993, p. 257.
36. J. P. Keener and J. Sneyd, *Mathematical Physiology*, Springer, New York, 1998.
37. S.K. Kim and D. Kaiser, *Science* **249**, 926 (1990).
38. S. Kim and D. Kaiser, *J. Bacteriol.* **173** (1991), p. 1722.
39. Kiskowski, M.A., M.S. Alber, Thomas, G.L., Glazier, J.A., Bronstein, N., Pu, J., and Newman, S.A., *Dev. Biol.* **271**, 372 (2004).
40. M.A. Kiskowski, *Discrete Stochastic Models for Morphological Pattern Formation in Biology*, Ph.D. Thesis, University of Notre Dame (2004).
41. J. Kuner and D. Kaiser, *J. Bacteriol.* **151**, 458 (1982).
42. Leonard, C.M., Fuld, H., Frenz, D.A., Downie, S.A., Massagu, J., and Newman, S.A., *Dev. Biol.* **145**, 99 (1991).
43. F. Lutscher and A. Stevens, *Journal of Nonlinear Sciences* **12**, 619 (2002).
44. C. Ma, Y. Zhou, P.A. Beachy, and K. Moses, *Cell* **75**, 927 (1993).
45. A. Marée, *From pattern formation to morphogenesis: Multicellular coordination in Dictyostelium discoideum*, Ph.D. Thesis., Utrecht, University, the Netherlands (2000).
46. A.F.M. Marée and P. Hogeweg, *Proc. Natl. Acad. Sci. USA* **98**, 3879 (2001).
47. J. Martiel and A. Goldbeter, *Biophys. J.* **52**, 807 (1987); T. Hoffer, J.A. Sherratt, and P.K. Maini, *Proc. R. Soc. London B* **259**, 249 (1995).
48. M. Matsushita and H. Fujikawa, *Physica A* **168**, 498 (1990);
I. Golding, Y. Kozlovsky, I. Cohen, and E. Ben-Jacob, *Physica A* **260**, 510 (1998);
A. Komoto, K. Hanaki, S. Maenosono, J.Y. Wakano, Y. Yamaguchi and K. Yamamoto, *J. Theor. Biol.* **225**, 91 (2003).
49. J. Murray, *Mathematical Biology*, Springer-Verlag, New York, 2003.
50. S. Newman, *Bioessays* **18**, 171 (1996).
51. C. Ofria, C. Adami, T. C. Collier, and G. K. Hsu, *Lect. Notes Artif. Intell.* **1674**, 129 (1999).
52. H. G. Othmer, S. Dunbar, and W. Alt, *J. Math. Biol.* **26**, 263 (1988).
53. N.S. Panikov, *Microbial Growth Kinetics*, Chapman and Hall, London, 1994.
54. R. Potts, *Proc. Cambridge Phil. Soc.* **48**, 106 (1952).

55. H. Reichenbach, in M. Dworkin and D. Kaiser (Eds.), *Mycobacteria II*, American Soc. Microbio., Washington DC, 1993.
56. P. Sahni, G. Grest, M. Anderson, and D. Srolovitz, *Phys. Rev. Lett.* **50**, 263 (1983); D. Srolovitz, M. Anderson, G. Grest, and P. Sahni, *Scripta Met.* **17**, 241 (1983).
57. E.M. Scott, E.A.S. Rattray, J.I. Prosser, K. Killham, L.A. Glover, J.M. Lynch, M.J. Bazin, *Soil Biol Biochem.* **27**, 1307 (1995).
58. L.J. Shimkets, R.E. Gill and D. Kaiser, *Proc. Natl. Acad. Sci. USA* **80**, 1406, (1983); S.K. Kim and D. Kaiser, *J. Bacteriol.* **173**, 1722 (1991); S. Li, B. Lee and L.J. Shimkets, *Genes Dev.* **6**, 401 (1992).
59. M. Steinberg, *Science* **137**, 762 (1962).
60. A. Stevens, *SIAM J. Appl. Math.* **61**, 172 (2000).
61. L. Tsimring, H. Levine, I. Aranson, E. Ben-Jacob, I. Cohen, O. Shochet, and W.N. Reynolds, *Phys. Rev. Lett.* **75**, 1859 (1995).
62. O. Wanner, *Biofouling* **10**, 31 (1996).
63. J. Wartiovaara, M. Karkinen-Jääskeläinen, E. Lehtonen, S. Nordling, and L. Saxén, *Progress in Differentiation Research*, North-Holland Publishing Company, Amsterdam, 245 (1976).
64. J. Wimpenny in C.R. Bell, M. Brylinsky, and P. Johnson-Green (Eds.), *Microbial Biosystems: New Frontiers Proceedings of the 8th International symposium on Microbial Ecology*, Atlantic Canada Society for Microbiol Ecology, Halifax, Canada (1999).
65. D. Wolf-Gladrow, *Lattice-gas cellular automata and lattice Boltzmann models - an introduction*, Springer-Verlag, Berlin, Lecture Notes in Mathematics, **1725** (2000).